Topographic Arrangement of the Rotundo-entopallial Projection in the Pigeon (*Columba livia*)

Felipe Fredes, Sebastian Tapia, Juan Carlos Letelier, Gonzalo Marín, and Jorge Mpodozis*

Facultad de Ciencias, Departamento de Biología, Universidad de Chile, Santiago, Chile

ABSTRACT

The tectofugal pathway (retina – optic tectum – nucleus rotundus – entopallium) is a prominent route mediating visual discrimination in diurnal birds. Several lines of evidence have shown that at the tecto-rotundal stage this pathway is composed of multiple parallel channels. Anatomical studies show that the nucleus rotundus is composed of at least four subdivisions, according to differences in cytoarchitectonic, histochemical, and hodological properties. Each of these subdivisions is in receipt of a highly convergent, nontopographic tectal projection, originating from a distinct subset of tecto-rotundal neurons. Physiological studies show that neurons of different subdivisions respond specifically to different visual dimensions, such as color, luminance, two-dimensional motion, and in-depth motion. At present it is less clear whether or to what extent this channel segregation is preserved at the telencephalic stage of the tectofugal pathway. The entopallium shows no obvious subdivisions or laminations. Nevertheless, tract-tracing experiments show that separate portions of the entopallium receive efferent projections from different rotundal subdivisions, in a way that maintains the rostrocaudal order of these subdivisions. In the present study we investigate in detail the topography of the rotundo-entopallial projection by means of anterograde and retrograde neuronal tracers. Our results confirm the zonal topography proposed by previous studies and indicate that each zone in the entopallium receives a direct and topographically organized projection from its corresponding rotundal subdivision. These results suggest that the spatial arrangement of the different rotundal functional modules is preserved at the entopallial level. J. Comp. Neurol. 518:4342–4361, 2010.

INDEXING TERMS: vision; birds; entopallium; rotundus; tectofugal; parallel visual pathways

The entopallium (E) is the largest visual structure in the telencephalon of most birds. It receives a major thalamic input from the nucleus rotundus thalami (Rt) through the fasciculus prosencephali lateralis (FPL; Karten and Hodos, 1970). The Rt, in turn, receives a visual input from the optic tectum (TeO; Karten and Revzin, 1966). The visual route from the retina through TeO and Rt to the entopallium is called the visual collothalamic (Butler, 1994) or the tectofugal pathway (Karten and Revzin, 1966; Karten and Hodos, 1970).

The tectofugal pathway is the main route mediating visual discrimination in most diurnal birds. Lesions in any of the structures of this pathway result in serious deficits in various visual tasks, such as brightness, color, pattern, spatial frequency, and size stimuli discriminations (Hodos and Karten, 1966, 1970, 1974; Cohen, 1967; Hodos and Bonbright, 1974; Macko and Hodos, 1984; Hodos et al., 1984, 1986, 1988; Kertzman and Hodos, 1988, Bessette and Hodos, 1989). Several lines of evidence have shown that at the tecto-rotundal stage the tectofugal pathway is composed of multiple parallel channels (Granda and Yazulla, 1971; Jassik-Gerschenfeld and Guichard, 1972; Yazulla and Granda, 1972; Frost and DiFranco, 1976; Wang and Frost, 1992; Wang et al., 1993; Karten et al., 1997; Laverghetta and Shimizu, 1999; Hellman and Gunturkun, 2001; Nyugen et al., 2004). In fact, in pigeons the Rt is composed of at least four main anatomical subdivisions (pars dorsalis anterioris [RtDa], pars Centralis [RtCe], pars Posterioris [RtPost], and pars Triangularis [RtTr]) distinguishable based on regional differences in cytoarchitectonic, histochemical, and hodological properties (Benowitz and Karten, 1976; Nixdorf and Bischof, 1982; Martinez-de-la-Torre et al., 1990; Mpodozis et al.,

Grant sponsor: Fondecyt; Grant numbers: 1030522, 1080094, 1080220.

*CORRESPONDENCE TO: Jorge Mpodozis, Departamento de Biología, Facultad de Ciencias, Universidad de Chile, Las Palmeras 3425, Ñuñoa, Santiago, Chile. E-mail: epistemo@uchile.cl

Received January 15, 2010; Revised April 15, 2010; Accepted June 19, 2010

DOI 10.1002/cne.22460

Published online July 26, 2010 in Wiley Online Library (wileyonlinelibrary.com)

1996; Redies et al., 2000; Hellman and Gunturkun, 2001; Marín et al., 2003). Each of these subdivisions is in receipt of a highly convergent, nontopographic tectal projection, originating from a distinct subset of tecto-rotundal neurons. (Benowitz and Karten, 1976; Nixdorf and Bischof, 1982; Martinez-de-la-Torre et al., 1990; Mpodozis et al., 1996; Karten et al., 1997; Redies et al., 2000; Hellmann and Guntunkun, 2001; Marin et al., 2003). Furthermore, the Rt subdivisions seem to have functional significance, as physiological studies show that neurons in different regions of the Rt respond specifically to different visual dimensions, such as color, luminance, two-dimensional motion, and in-depth motion (Wang et al., 1993).

At present it is less clear whether or to what extent this channel segregations is preserved at the telencephalic stage of the tectofugal pathway. The entopallium shows no obvious subdivisions or laminations on the basis of cytoarchitecture (Rehkamper et al., 1985), morphology (Tömböl, 1991), or the distribution of several neurochemicals (Brauth et al., 1986; Dietl and Palacios, 1988; Dietl et al., 1988a,b; Veenman and Reiner, 1994; Veenman et al., 1994; Hellmann et al., 1995). Nevertheless, tract-tracing experiments show that separate portions of E receive efferent projections from different subdivisions of Rt, in a way that maintains the rostrocaudal order of the rotundal subdivisions (Benowitz and Karten, 1976; Nixdorf and Bishof, 1982; Laverghetta and Shimizu, 2003; Krützfeldt and Wild, 2005). Furthermore, behavioral experiments show that bilateral lesions in the caudal or the rostral entopallium of trained pigeons results in differential discrimination deficits for motion or grating task, respectively (Nguyen et al., 2004). These results suggest that there is an anatomical and functional segregation in the entopallium that could reflects the channel segregation present in Rt.

Two previous anatomical studies (Krützfeldt and Wild, 2004, 2005) have indicated heterogeneity within the E. These studies reveal a dorsoventral partition in the E, which differs substantially in terms of their afferent and efferent projections. The internal (ventral) part of E shows reciprocal projections with the nucleus mesopallialis ventrolaterale (MVL), it is the sole source of entopallial projections to the striatum, and hence appears to be closely related to extratelencephalic circuits. The external (dorsal) part, instead, receives denser rotundal projections and most probably projects to several nidopallial areas. This evidence implies that the different divisions or channels in the tectofugal pathway diverge at the level of entopallial efferents.

In the present study we investigate in detail the topography of the rotundo-entopallial projection by means of anterograde and retrograde neuronal tracers. Our results confirm the zonal topography proposed by Laverghetta and Shimizu (2003) and indicate that each zone in the entopallium receives a direct topographically organized projection from its corresponding rotundal subdivision. These results suggest that the spatial arrangement of the different functional modules present at the rotundal level is preserved by the rotundo-entopallial projection.

MATERIALS AND METHODS

This study used a total of 22 wildtype adult pigeons (*Columba livia*), 300–350 g in body weight, of both sexes. These animals were obtained from a local dealer and kept in an institutional animal facility with a 12-hour light/dark cycle and free access to water and food. All the experimental procedures were approved by the Science Faculty's Ethics Committee (Comité de Ética de la Facultad de Ciencias de la Universidad de Chile) and conformed to the guidelines of the National Institutes of Health (NIH) on the use of experimental animals in research.

The pigeons were deeply anesthetized by means of an intramuscular injection of ketamine (40 mg/kg body weight) and xylazine (12 mg/100 kg body weight). Then the animals were mounted in the standard stereotaxic position (Karten and Hodos, 1967) in a custom-designed head holder that did not interfere with the animal's visual field. Thereafter, the skull was exposed through a skin incision, and a craniotomy was made to expose the dorsal telencephalon above the approximate location of either the nucleus Rt or the entopallium, depending on the experiment. Injections of different tracers were then made into these structures according to the procedures described below. After the injections the wounds were covered, the skin sutured, and treated with topical antibiotics. During the experiment the heart rate of the animals was continuously monitored and the body temperature was held at 40–42°C by means of a thermoregulated electric blanket. During surgery and recovery all wounds and pressure points were treated with a commercial ointment of 5% lidocaine. When necessary, supplementary doses of anesthetic (0.2 mL every 2 hours) were given to the animals.

In a first set of experiments the fluorescent, lipophilic tracers DiI and True Blue (TB) were injected into the left entopallium of 18 animals. In four of these cases each animal received a single injection of either DiI (two cases) or TB (two cases). In 14 cases the animals received two injections, one of each tracer. In an attempt to produce small, well-defined injections and to minimize tracer diffusion, the tracers were injected in their solid, crystalline form by means of a "solid microinjector" apparatus (Marin et al., 2001). Briefly, this consists of a blunt 36G hypodermic needle, equipped with a movable internal rod, which is connected to a syringe-like pressure chamber. When a gas pressure pulse is applied to the chamber, the rod moves forward and back inside the needle, pushing out a solid load previously packed inside the needle tip. To perform

the injections we first identified the entopallium by its electrophysiologically recorded responses to visual stimuli presented to the contralateral eye. Electrophysiological signals were recorded with 1 MΩ impedance tungsten electrodes, amplified (AM Systems, Everett, WA; model 1800) and monitored in an oscilloscope (Tektronix, Beaverton, OR; 5113) coupled to an audio monitor. Visual responses were elicited stimulating the contralateral visual field with a hand-held laser pointer. Once the entopallium was electrophysiologically identified, the electrode was replaced by the loaded microinjector, following the coordinates obtained in the recording session. The injections were made by applying a train of pressure pulses, according to previously determined parameters (for details, see Marin et al., 2001). The pressure source was an N2 tank at 1,000 psi, and the pressure drive was a custom-made picospritzer device. After 3–5 minutes the microinjector was slowly withdrawn. In a separate set of experiments the anterograde tracer biotinylated dextran amine (BDA 10,000 MW, Invitrogen, Carlsbad, CA) was injected into the nucleus rotundus of both hemispheres in order to perform two separate experiments in one animal. To accomplish this, glass micropipettes of 10–15 μm tip diameter were filled with a 10% solution of 10,000 Mr biotinylated dextran amine (BDA; Molecular Probes, Eugene, OR) in 0.01 M phosphate buffer. Then the pipette was positioned and advanced at the stereotaxic coordinates obtained in a previous electrophysiological recording, as described for the entopallium. The injection was made by applying a train of pressure pulses, as described above. After 5–9 days of survival, the animals were deeply anesthetized with an overdose of a mixture of ketamine and xylazine and perfused via the aorta with 500–800 mL of 0.9% saline, followed by 1,000 mL of an ice-cold solution of 4% paraformaldehyde in 0.1 M phosphate buffer (pH 7.2). After the perfusion the brains were excised, postfixed overnight in the paraformaldehyde solution, and then transferred for 1–2 days to a 30% sucrose solution for cryoprotection. The brains were then mounted in the stereotaxic plane over the stage of a frozen sliding microtome and 60 μm sections were cut in the sagittal or transverse plane. In the cases with injections of fluorescent tracers the sections were immediately mounted in avian saline. In the cases with BDA injections the collected tissue was washed for 30 minutes in phosphate-buffered saline (PBS) and then reacted with an avidin-biotin reagent (ABC Elite Kit, Vector Laboratories, Burlingame, CA) in 0.3% Triton X-100 in PB for 1 hour. Sections were then washed in PBS and reacted in 0.025% diaminobenzidine (DAB, Sigma, St. Louis, MO) and 0.3% hydrogen peroxide in PB for 20 minutes. Sections were mounted on glass slides, dehydrated in an ethanol/xylene series, and coverslipped with Permount (Fisher Scientific, Fair Lawn, NJ). In all cases, selected sections or series of sections were counterstained with cresyl violet for further analysis.

The sections were examined and photographed using a conventional epifluorescent microscope (Olympus Bx 60) with a digital color camera and associated software (Spot Digital Camera; Diagnostic Instruments, Sterling Heights, MI). To study the location, distribution, and intensity of the fluorescent retrogradely labeled cells in the nucleus rotundus, a series of microphotographs was taken of every third section. Depending on the tracer used, the digital images were taken with the blue or red channel, setting the camera exposure time in a way that the more intensely labeled cells just reached the highest pixel value (255), which was then used for all photographs of a given case. The photographs were transferred to Adobe Photoshop CS3 (Adobe Systems, Mountain View, CA) and combined to reconstruct views of the whole sections. As only two different tracers were used in these experiments, color was not essential in order to display the results. Thus, both channels were transformed to gray scale, and the red channel was inverted in contrast, in such a way that the red cells appeared black and the blue cells appeared white in the final reconstructed image. The shape and trajectory of anterograde labeled rotundal axons inside the entopallium were reconstructed in drawings based on serial sections using a camera lucida attached to the microscope. Once the fibers were reconstructed the drawings were scanned and the digital version obtained. For all nonfluorescent figures minor aesthetic manipulations such as contrast and white balance corrections were carried out in Adobe Photoshop CS3.

RESULTS

Boundaries and subdivisions of the entopallium

Krützfeldt and Wild (2005) observed in pigeons that the E is readily distinguishable in the transverse plane as a zone of higher opacity in unstained, wet-mounted tissue. We reproduced these observations and confirmed that the limits of the E were comparable to those described in the transverse plane in the pigeon stereotaxic atlas (Karten and Hodos, 1976) (Fig. 1B). We then carried out similar observations in a series of parasagittal wet-mounted sections. This allowed us to better define the limits of the E at the most lateral and medial parasagittal levels (Fig. 1A). None of these observations gave evidence of a rostrocaudal partition of E. We then attempted to delimit the E by labeling its rotundal afferences. To that end we performed a triple BDA injection into Rt, aimed to fill the whole extent of the nucleus. The tracer spread to some other structures of the dorsal thalamus, such as the OPT (not shown), which are not relevant for this study,

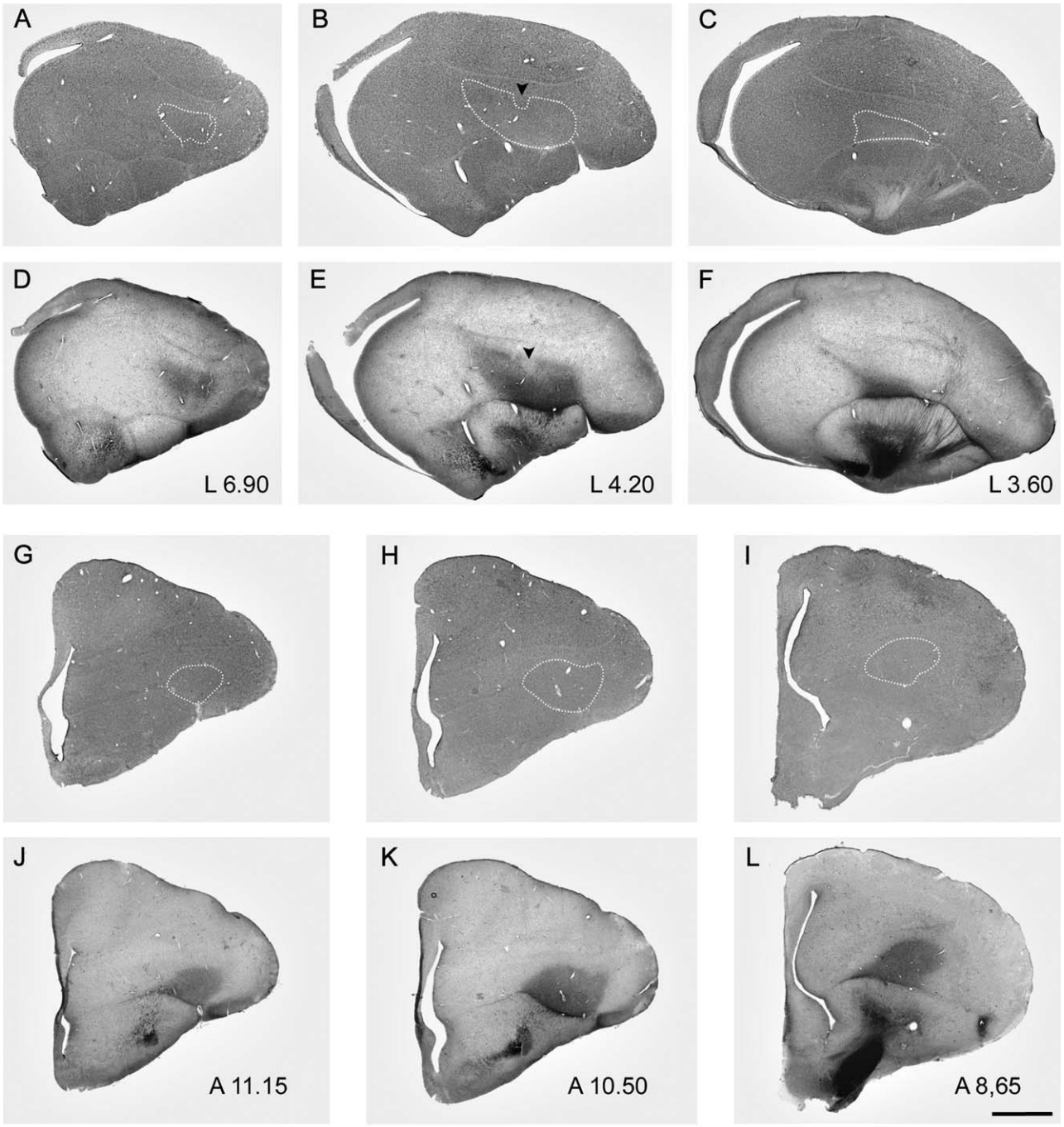

Figure 1. Differential opacity of the entopallium in fixed, wet tissue. **D–F**: Sagittal, **J–L**: transverse sections through the telencephalon mounted in water. Note the central high opacity zone corresponding to the entopallium (E). **A–C,G–I**: The same sections stained with Nissl. The E is outlined in the Nissl sections with a dotted line following the high opacity zone of the wet sections. Note the indentation indicated with an arrowhead (B,E). The approximate rostrocaudal and lateromedial stereotaxic coordinates in accordance with the pigeon stereotaxic atlas (Karten and Hodos, 1977) are indicated in the right inferior corner of the pictures. Scale bar = 1 mm.

as the Rt is the only known source of thalamic projections to the E (Benowitz and Karten, 1976). The results of these injections revealed, in the sagittal plane, a very dense field of labeled terminals (Fig. 2) that closely matched the entopallial limits previously revealed from the wet tissue (Fig. 1). A more detailed analysis of the pattern of labeling suggests a rostrocaudal subdivision of E into three different partitions, defined by a differential density of the rotundal terminals. The anterior partition appears as a polygonal, drop-shaped area, clearly discernible from the more caudal regions by the higher density of its rotundal afferents, especially evident at lateral levels (Fig. 2A,B).

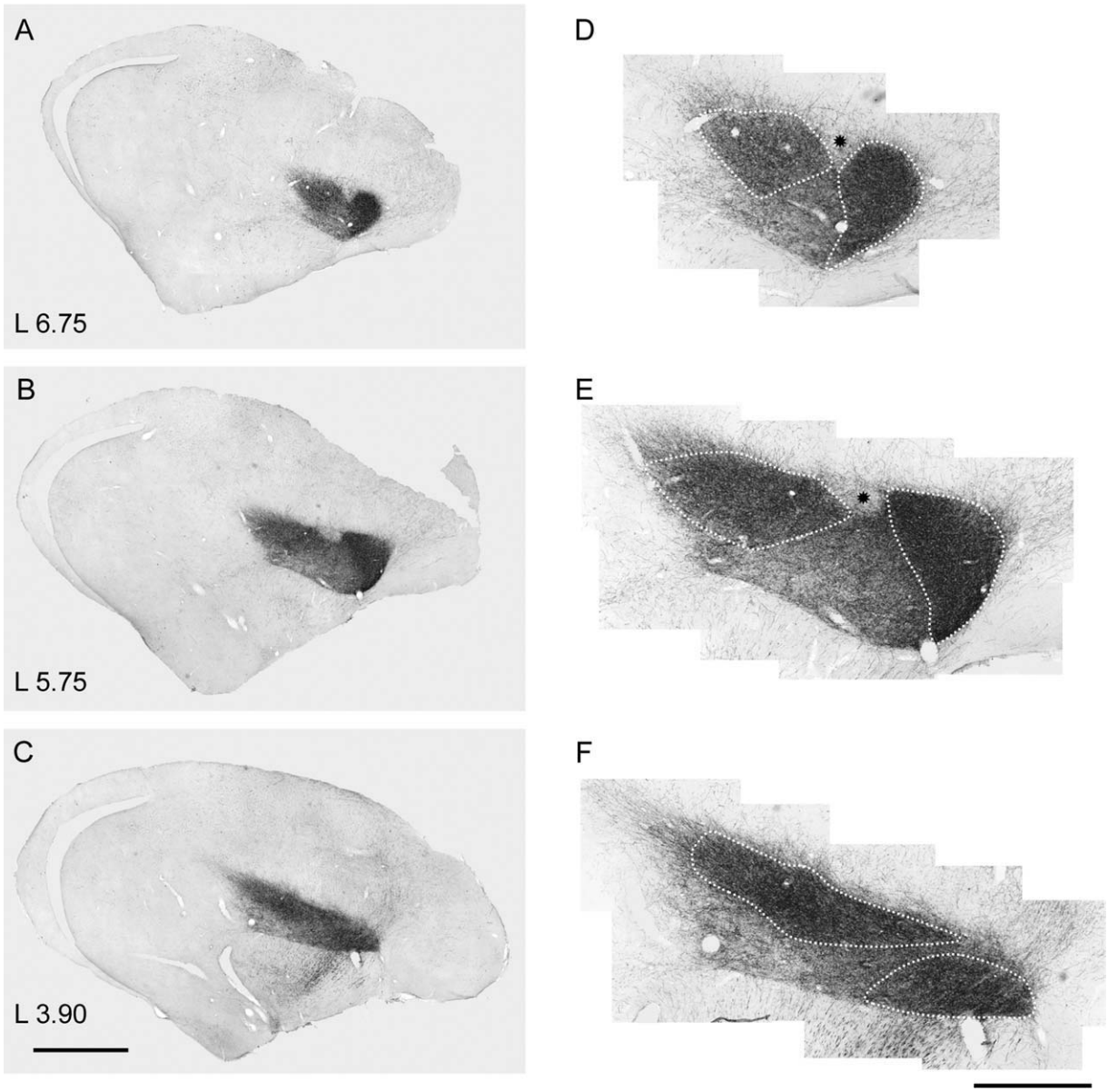

Figure 2. Anterogradely labeled fibers from the Rt delimit three zones in the entopallium. **A–C**: Sagittal sections at different lateromedial coordinates, showing dense terminal fields after a large BDA injection in the ipsilateral nucleus rotundus. **D–F**: Higher magnification of the entopallial zones of the sections on the left. The caudal and rostral zones, which appear innervated by a higher density of rotundal terminals, are outlined by broken lines. Note in the dorsomedial aspect of the E the presence of a region with very low density of terminals (indicated by the asterisks). Rostral is to the right and caudal to the left. The approximate lateromedial stereotaxic coordinates in accordance with the pigeon stereotaxic atlas (Karten and Hodos, 1977) are indicated in the right inferior corner of A–C. Scale bars, left column = 1 mm; right column = 2 mm.

The central partition exhibited a relatively minor density of label, and appeared as a trapezoid, "volcanic cone," with its basis lying on the ventral pallial/striatal boundary and a narrow apex oriented anterodorsally (Fig. 2B). The posterior partition also presented a high density of labeled terminals, and appeared as a lenticular area encompassing the dorsal posterior crescent of E. This partition also dorsally embraced the central area of the E in the rostrocaudal axis (Fig. 2C).

Zonal topography in the rotundo-entopallial projection

We sought to confirm the existence of these partitions and to investigate a possible relation between them and the rotundal subdivisions. For this purpose we carried out a series of experiments aimed at locating BDA injections in each of the rotundal subdivisions. In the first experiment the BDA injection was localized in the rostral part of the dorsal thalamus. Notwithstanding the large size of the

deposit, only the dorsal anterior subdivision (Da) of the rotundus was injected. This experiment resulted in the anterograde labeling of a drop-shaped region, a region that closely matched the anterior partition of E described above. No other labeling could be seen in the E (Fig. 3E,F). In this case a bundle of labeled fibers that seems to leave the E in an oblique direction towards the dorsal anterior telencephalon was also clearly visible. These fibers likely originate from the thalamic OPT, which was also involved in the tracer deposit. In a subsequent experiment we performed a BDA injection into the ventral portion of the central Rt (Fig. 3C). This injection resulted in a dense field of anterogradely labeled axons mainly restricted to the ventral part of the central partition of E. Some labeled axons were also located in the posterior partition, probably as a consequence of the spread of tracer to the posterior Rt. The anterior partition of the E appeared largely free of terminals (Fig. 3D). In the next experiment we performed an injection that affected mainly the dorsal moiety of the central Rt. In this case some of the tracer also spread to the posterior subdivision, as shown in Figure 3A. This injection resulted in dense labeling of a patch of terminals mainly located within the dorsal aspect of the central partition of E. The labeled fibers extended also rostrally and caudally from this locus. The anterior partition of E, as well as the ventral half of it, was free of significant label (Fig. 3B). Finally, we carried out a BDA injection in the posterior division of Rt. Although the tracer diffusion reached partially the central Rt, the field of anterograde labeled fibers was mostly circumscribed within the limits of the posterior partition of E (compare Fig. 3A,C). The labeled terminals also extend to the ventral zone of the central partition, probably as a consequence of the tracer diffusion to the Ce (Fig. 3G,H). No labeled fibers were observed in the anterior or dorsal E. These results confirm the existence of a zonal organization in the rotundo-entopallial projection, as proposed by other authors (Benowitz and Karten, 1976; Nixdorf and Bishof, 1982; Laverghetta and Shimizu, 2003; Krützfeldt and Wild, 2004), and suggest that each subdivision of the Rt projects to a specific domain of E, in a way that preserves the rostrocaudal order of the rotundal subdivisions.

Topography in the rotundo-entopallial projection

In the previous experiments we observed that BDA injections into the dorsal and ventral portions of central Rt resulted in a differential dorsoventral pattern of labeling in the E. This prompted us to ask about the possible presence of a topographic arrangement within the projection from a given rotundal subdivision to its recipient entopallial zone. To answer this question we performed a series of minute injections of liposoluble retrograde tracers (DiI and True Blue), injected in crystalline form to avoid the diffusion of the tracers. The size of the injected crystals did not exceed 50 μm in diameter. In a first set of experiments we performed two separate injections, one of True Blue and the other of DiI, into the rostral aspect of E. Figure 4 shows the injection site and the location of the retrogradely labeled cells in a representative case. In this case the True Blue crystal was located closer to the lateral part of the nucleus, while the DiI crystal was positioned closer to its medial border. As a result of these injections, retrogradely labeled neuronal cell bodies were located exclusively in the dorsal anterior rotundal subdivision (Da). Furthermore, it was possible to distinguish two well-defined cell clusters in accordance with the transported tracer: those cells labeled with True Blue were located in the lateral region of Da, while those cells labeled with DiI were distributed closer to the medial region of Da. These clusters overlapped in the central region of Da, where some double-labeled cells were observed. In a second set of experiments we carried out double injections in the central region of E. Figure 5 shows a representative case, in which the True Blue crystal was located closer to the midline, while the DiI crystal was positioned 100 μm more lateral and ≈100 μm more ventral than the True Blue crystal. As expected, the clusters of retrogradely labeled cells were mostly located in the centralis subdivision of Rt, although some bodies were also observed in the posterior Rt and triangularis subdivision. As in the previous case, the two cell clusters were segregated in accordance with the type of crystals: the True Blue labeled cells were located lateroventrally within the Ce subdivision, while the somata labeled with DiI were located dorsomedially within the Ce. Some double-labeled cells were also observed distributed in the area of superimposed clusters. In the next set of experiments we performed double injections in the posterior partition of E. Figure 6 shows the results of a representative case, in which the True Blue crystal was located closer to the midline, while the DiI crystal was located 150 μm laterally and 100 μm ventrally. As expected, the resulting retrogradely labeled cells were exclusively located in the posterior subdivision of Rt. In accordance with the previous experiments, the labeled cells formed two well-defined cell clusters: the DiI-labeled cells were located in the ventrolateral region of Post, while the True Blue labeled somata were located in the dorsomedial part of Post.

Control experiments

The previous results suggest the existence of a fine topographic relation between the rotundal subdivisions and their corresponding entopallial partitions. To control for possible technical artifacts, we devised two different

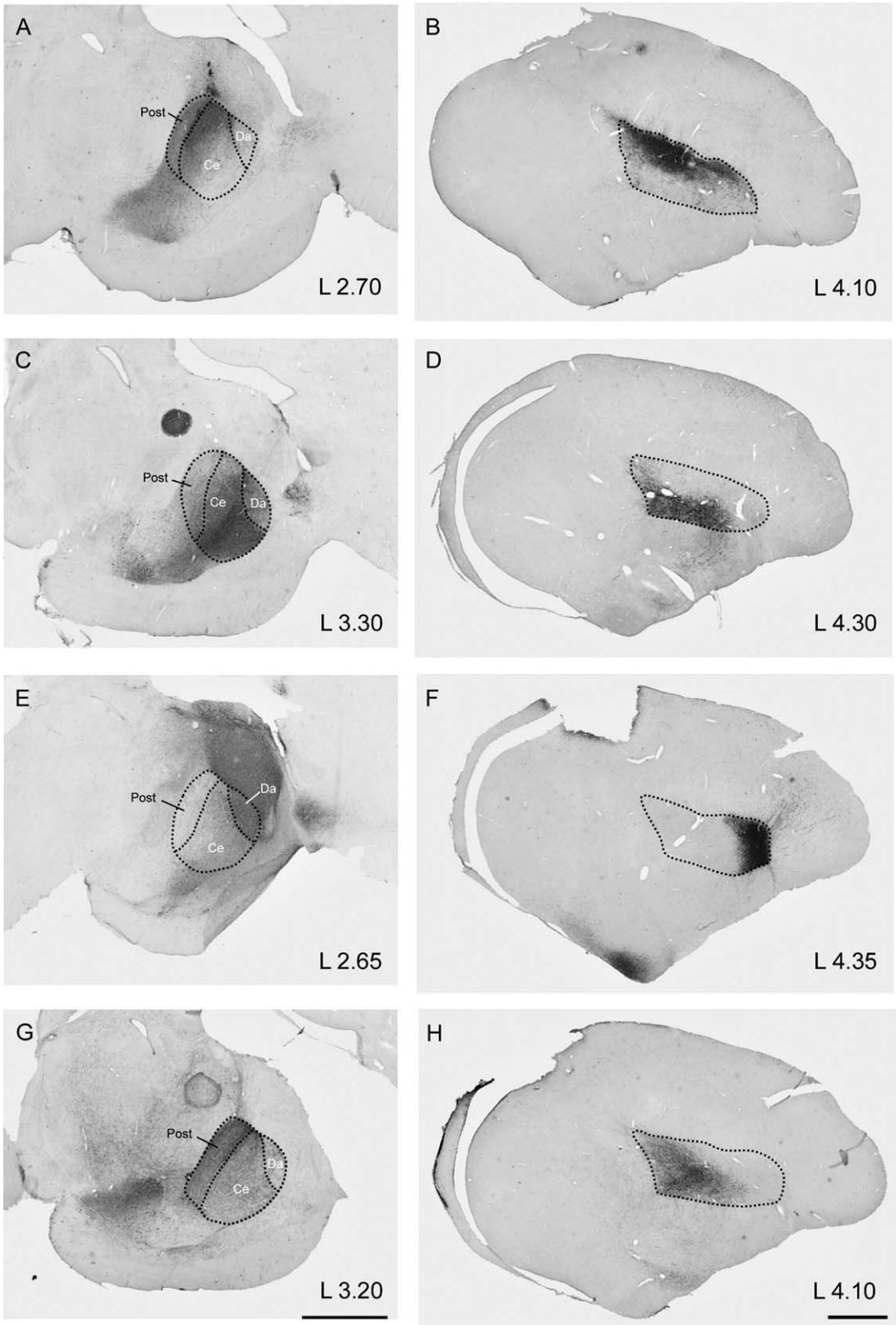

Figure 3. Zonal topography in the rotundo-entopallial projection. Sagittal sections showing BDA injection sites (left) and the resulting anterograde label in the E (right). **A,B**: An injection encompassing mainly the dorsal moiety of the central subdivision of Rt (Rt-Ce), with some diffusion of tracer into the posterior subdivision (Rt-Post), produces a termination zone confined to the dorsocaudal part of the E, while the rostral zone is completely free of label. **C,D**: An injection into the ventral moiety of Rt-Ce produces a termination zone confined to the ventral zone of the E. **E,F**: An injection encompassing the principal optic thalamic nuclei (OPT) and the dorsal anterior subdivision of the rotundus (Rt-Da) produces a termination zone only at the rostral part of the E. **G,H**: An injection into the Rt-Post, with some diffusion of tracer into the Rt-Ce produces a termination localized in the posterior and ventromedial region of the E. Scale bars = 1 mm.

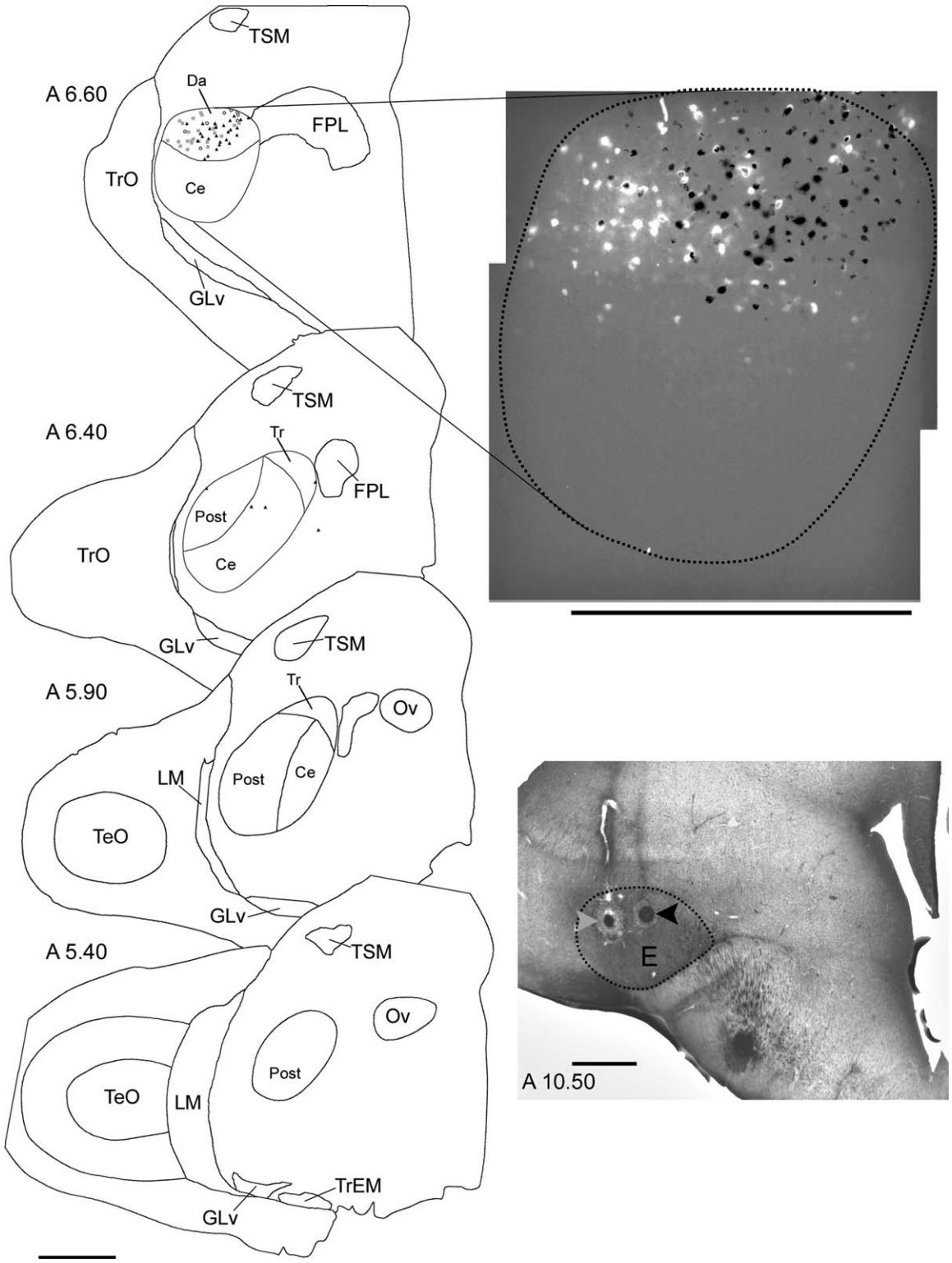

Figure 4. Distribution of labeled cells in dorsal anterior Rt, after a double injection of DiI and True Blue crystals in the rostral entopallium. **Left column**: Drawings of a series of transverse sections containing the rotundus, at different rostrocaudal coordinates. The cell bodies labeled with DiI and True Blue are represented as black triangles and gray squares, respectively; open circles indicate double-labeled cells. **Upper right**: Fluorescent microphotograph corresponding to the most anterior schematic is displayed on the right. In order to show the image in gray scale a contrast modification was carried out, such that the black and white colors correspond to the DiI and True Blue labeling, respectively. **Lower right**: Transverse section showing the position of the crystals in the rostral portion of the entopallium; the black and gray arrowheads indicate the DiI and True Blue crystals, respectively. Note that two clusters of labeled cells, displaced in the mediolateral axis, are found only in the dorsal anterior subdivision of the Rt. The approximate rostrocaudal stereotaxic coordinates in accordance with the pigeon stereotaxic atlas (Karten and Hodos, 1977) are indicated in the left side of each drawing and photograph. Scale bars = 1 mm.

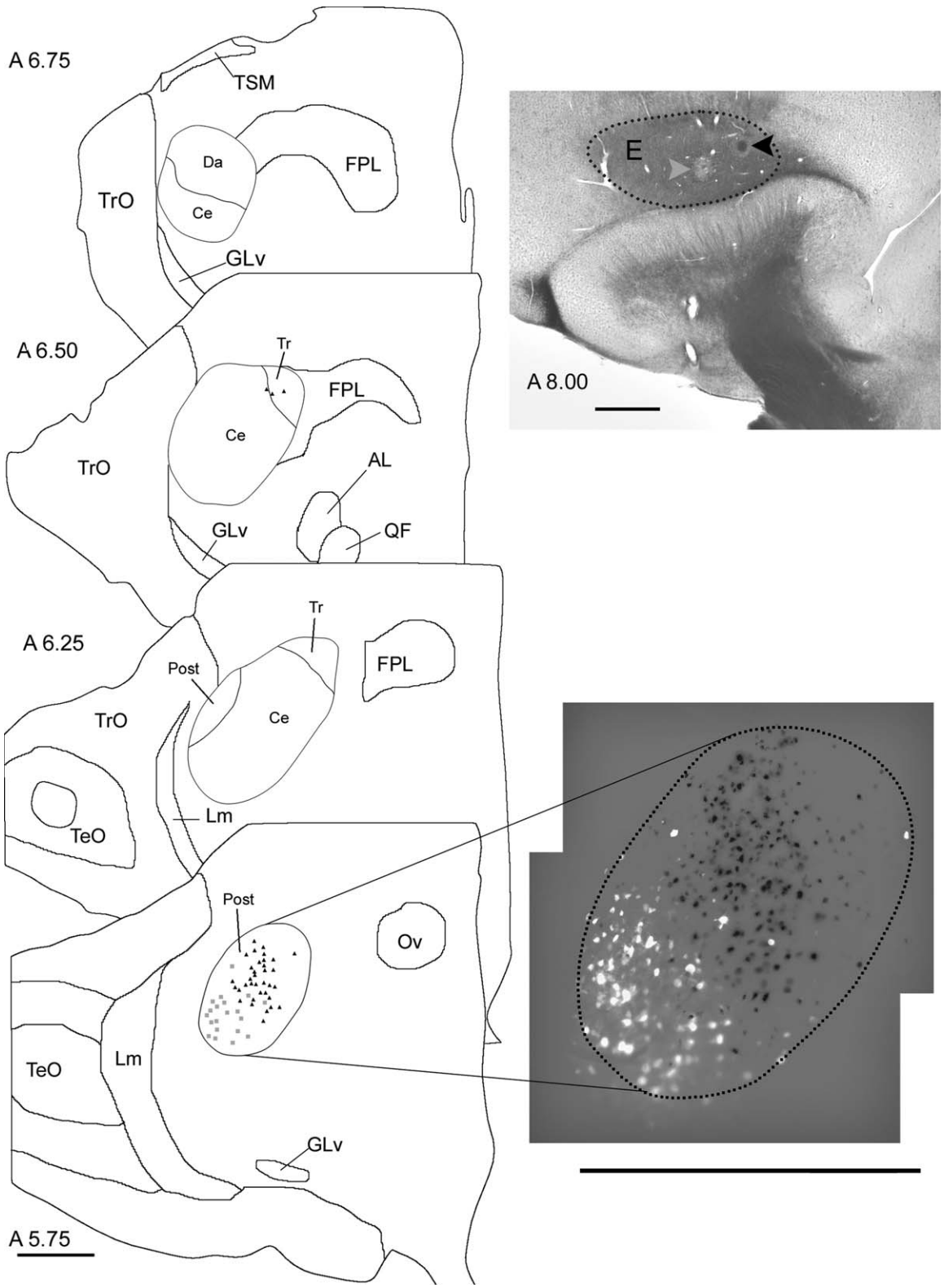

Figure 5. Double injection into the caudal zone of the E and the resulting retrogradely labeled cells in the Rt. Note that the cells are mainly located in the posterior Rt subdivision, with the only exception of three cells located in triangularis. Note also the topographic relation between the position of the labeled cellular clusters in the Rt and the location of the crystals in the E. Scale bars = 1 mm.

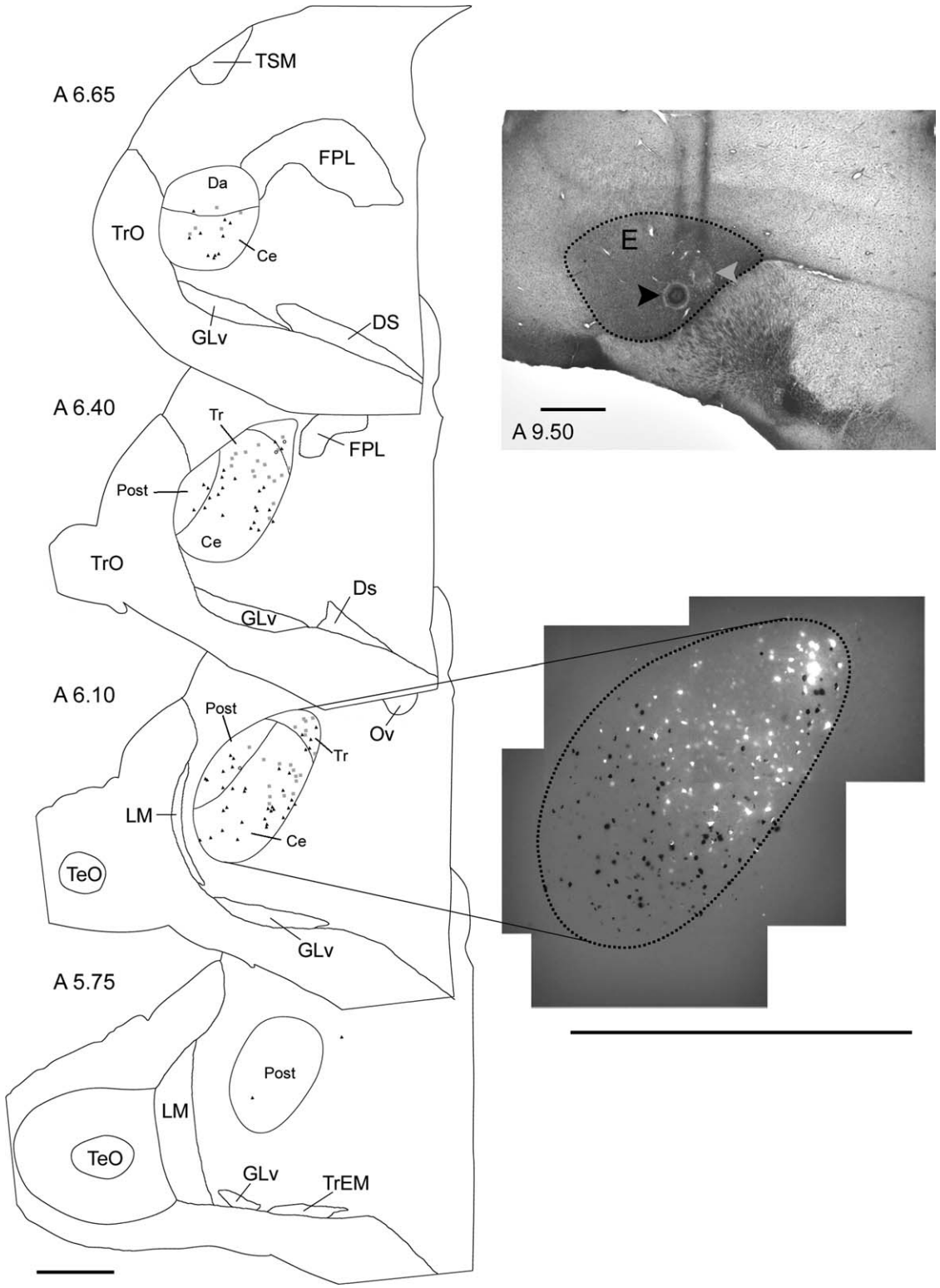

Figure 6. Double injection in the central zone of the E and the resulting retrogradely labeled cells in the Rt. Note that the labeled cells are mainly located in the Rt centralis. Note also that there is a topographic relationship between the position of the crystals in the E and the retrogradely labeled cell clusters. Scale bars = 1 mm.

experiments. A first control consisted of localizing crystals of DiI and True Blue as close as possible (50 μm) in the central region of E (Fig. 7). According to our previous experiments described above, this should result in closer and intermingled clusters of retrogradely labeled cells in Rt. As expected, the retrogradely labeled cells were

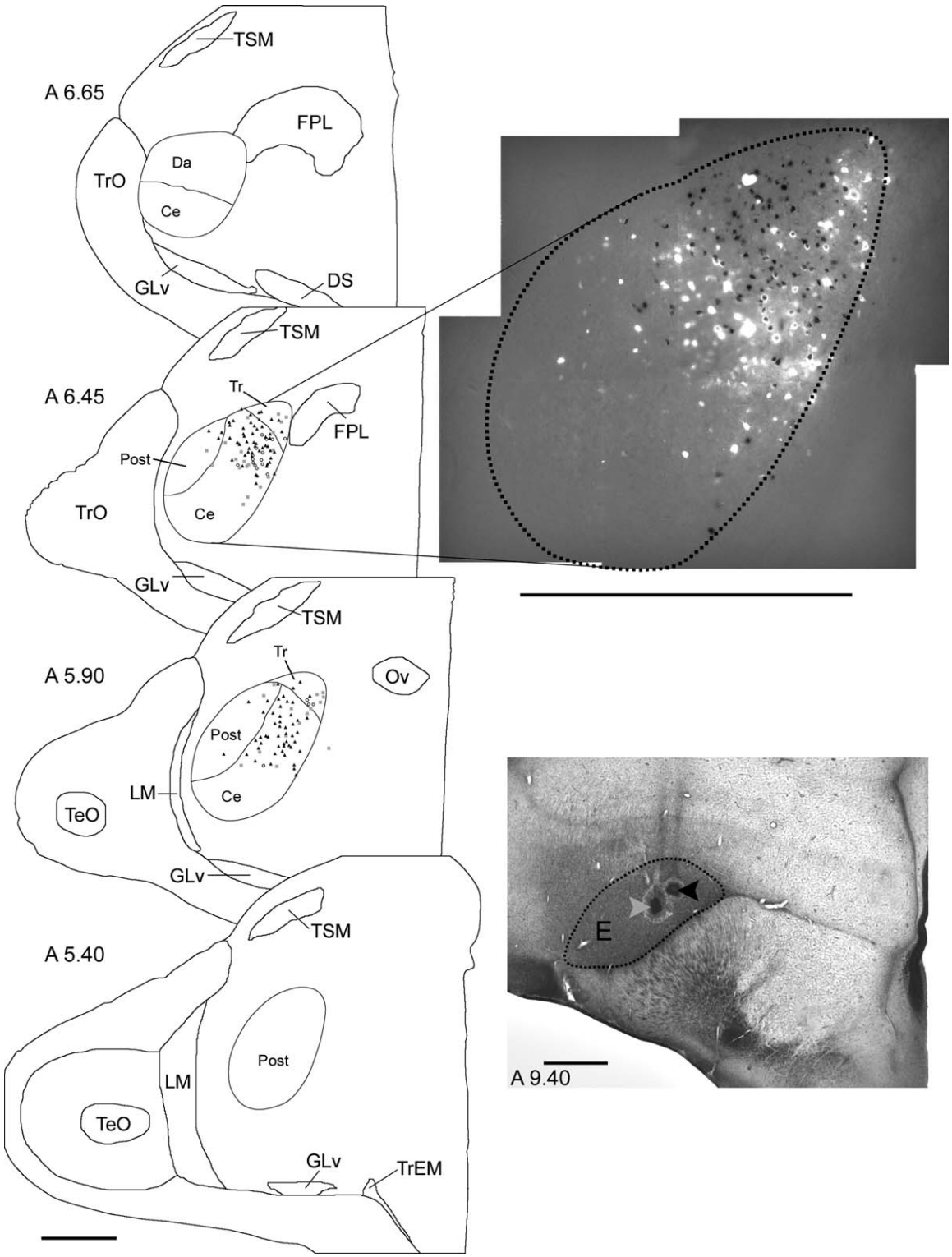

Figure 7. Closely located injections in the central region of the E and the resulting retrograde labeled cells in the Rt centralis and triangularis. The crystals are very close to each other and the diffusion halos are superimposed. Correspondingly, the labeled cell clusters in the Rt have a large superimposed area with a high proportion of double-labeled cells. Nevertheless, the cluster maintains their topographic relation with the position of the crystals in the E. Scale bars = 1 mm.

located mainly in the Ce subdivision of Rt, although some labeled cell bodies where also seen in the triangularis subdivision. The area where the two differentially labeled clusters of cells superimposed was much larger than in the previous cases and contained many double-labeled cells. However, even in this extreme case the location

and orientation of these clusters reflects the position of the crystals in the E, as the cells labeled with DiI tended to be located more dorsally than those labeled with True Blue (Fig. 7). A second control consisted in localizing the crystals as far apart as possible in the central region of E. This should result in two clearly distinct clusters of retrogradely labeled cells in Rt, with minimum overlap between them. In this instance the DiI crystal was located closer to the midline, while the True blue crystal was located 500 μm more lateral and 50 μm more ventral than the DiI one (Fig. 8). As expected, the retrogradely labeled cells were largely restricted to the central Rt and distributed in two clearly defined, differentially labeled clusters, with no overlapping boundaries. The position of these clusters correlated well with the position of the crystals in E, as the cells labeled with DiI were mainly located in the dorsal region of Ce, while the cells labeled with True Blue were located in the lateroventral region of Ce.

Topology of the rotundo-entopallial projections

To reveal more precisely the topological organization of the rotundo-entopallial projections, we attempted to correlate the position of the injection sites in E with the position of the resulting clusters of labeled cells in Rt. To that end, we first attempted to localize each of the injection sites in E, as well as each of the resulting clusters of labeled cells in Rt, in a 3-axis coordinate system. For the injection sites in the E, mediolateral and dorsoventral coordinates were estimated relative to the profile of the nucleus, according to the following procedure: first we measured the distance of the crystal's geometrical center to the medial, or dorsal, limit of the nucleus (e.g., the "b" distance in Fig. 9) and then we measured the total lateromedial, or dorsoventral, size of the nucleus (e.g., the "a" distance in the Fig. 9). The quotient between "b" and "a," that is, the normalized distance (d) of that crystal with respect to the medial or dorsal boundary of the E in that specific section, was used as the mediolateral or dorsoventral coordinate of each injection site. A similar procedure was applied to estimate the coordinates of the retrogradely labeled cell clusters in Rt. In this instance, the geometric center of each cluster was estimated as the center of the zone of maximum density of labeled cells. In both nuclei the anteroposterior coordinates of the relevant points were estimated from the stereotaxic atlas (Karten and Hodos, 1967), using the location of representative brain structures in each section as landmarks.

We used these values to generate nine plots correlating all possible axis combinations (Fig. 9). The correlation coefficients were statistically significant (Pearson Product-Moment Correlation Coefficient Table, $P > 0.05$) only for the correlations between the lateromedial axis in the Rt vs. the lateromedial axis in E ($n = 18$, $r = 0.45$), and the rostrocaudal axis in Rt with the rostrocaudal axis in E ($n = 11$, $r = 0.55$). The correlation between the dorsoventral axis in Rt vs. dorsoventral axis in E approached significance ($n = 17$, $r = 0.412$), but all other regressions (all other combinations of axes) yielded insignificant correlation coefficients (not shown).

Arborization of the rotundal terminals in the E

To determine the shape and area of arborization of the rotundal terminals in E, we attempted to anterogradely label single rotundal fibers by means of small pressure injections of BDA in the Rt. Due to the limitations of this technique, only in a few instances were we able to observe reasonably well-isolated rotundal axons. In the best of our cases, the BDA injection was located in the dorsalmost part of Da (not shown). In accordance with our previous results, we found a single labeled axon in the dorsal part of the anterior zone of the E (Fig. 10). We proceeded to a camera lucida reconstruction of all sections in which parts of the axon were distinguishable, in all focal planes. The reconstruction shows that after entering the E, the principal branch of the axon follows a straight ventral-to-dorsal course for about 100 μm, without leaving synaptic buttons or varicosities, until it reached the point of bifurcation where two thinner branches appeared and began to generate fine arborizations, leaving profuse varicosities as they climbed dorsally (Fig. 10, superior row). In accordance with our double injection results the arborization span of this axon was no more than 150 μm. Similar morphological characteristic were observed in all other cases in which we obtained reasonably well-labeled single axons (Fig. 10, inferior row).

DISCUSSION

Zonal topography in the rotundo-entopallial projection

Several previous studies have shown that each of the different subdivision of Rt projects to a definite region of E, in such a way that the rostrocaudal order of the rotundal subdivisions is maintained in the corresponding entopallial regions (Benowitz and Karten, 1976; Nixdorf and Bishof, 1982; Laverghetta and Shimizu, 2003; Krützfeldt and Wild, 2004). We sought to confirm the existence of this zonal topography, and to investigate if there is a correspondence between the entopallial projection zones of each of the rotundal subdivisions and the rostrocaudal partitions suggested in our previous experiments. For this purpose we carried out small BDA injections localized in each rotundal subdivision, and then processed the tissue

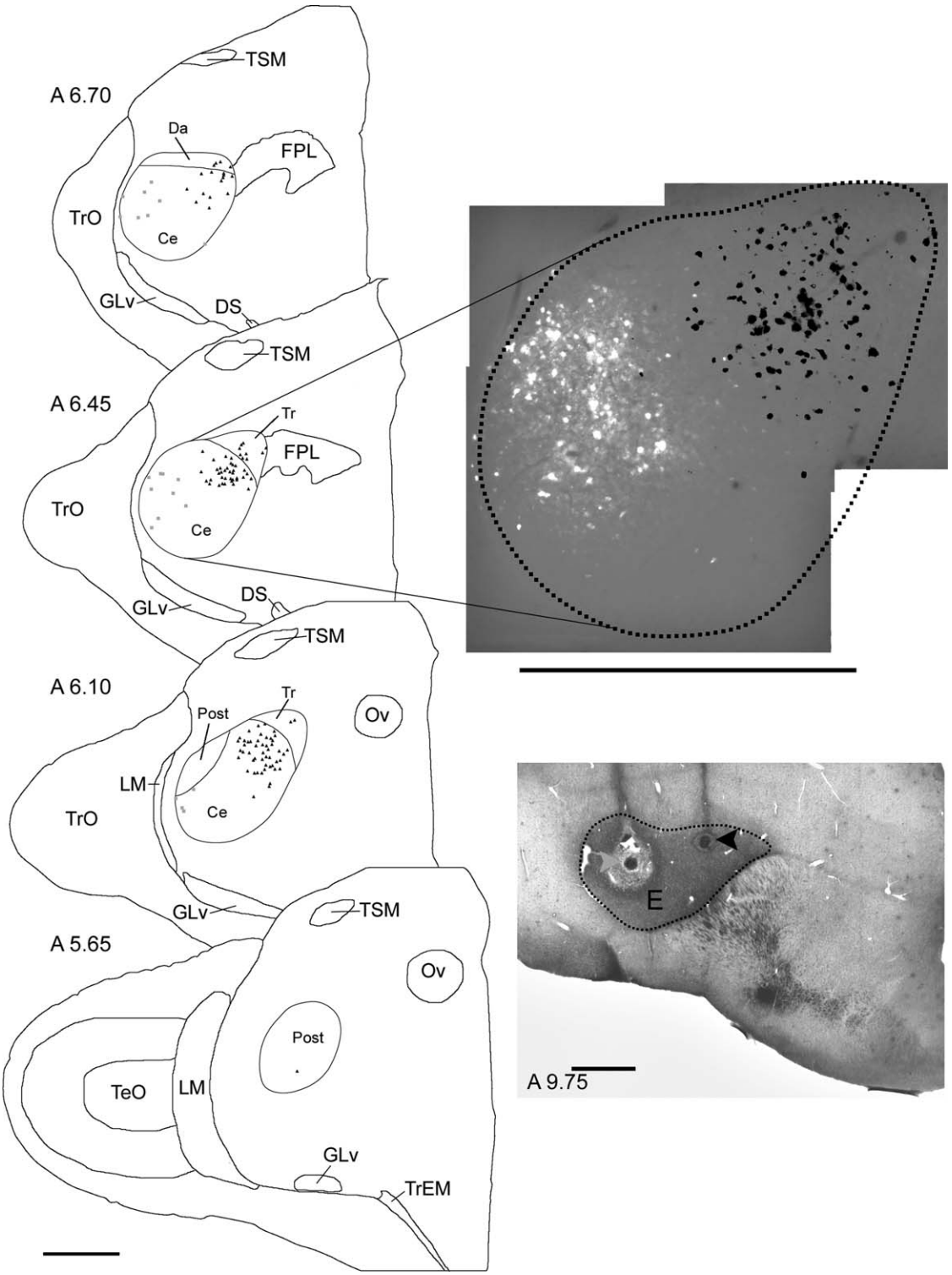

Figure 8. Well-separated injections in the central region of the E and the resulting retrogradely labeled cells in the Rt centralis and triangularis. The crystals are separated by ≈500 μm from each other. Note that there are no double-labeled cells and the labeled cells clusters are separated by at least 100 μm. The distribution of the labeled cell clusters corresponds to the topographic location of the crystals in E. Scale bars = 1 mm.

in the sagittal plane. The results of these experiments readily confirm the zonal topography, as they show that each of the rotundal subdivisions projects to a different region of E, and that these regions succeed each other rostrocaudally in the same order as their corresponding Rt subdivisions.

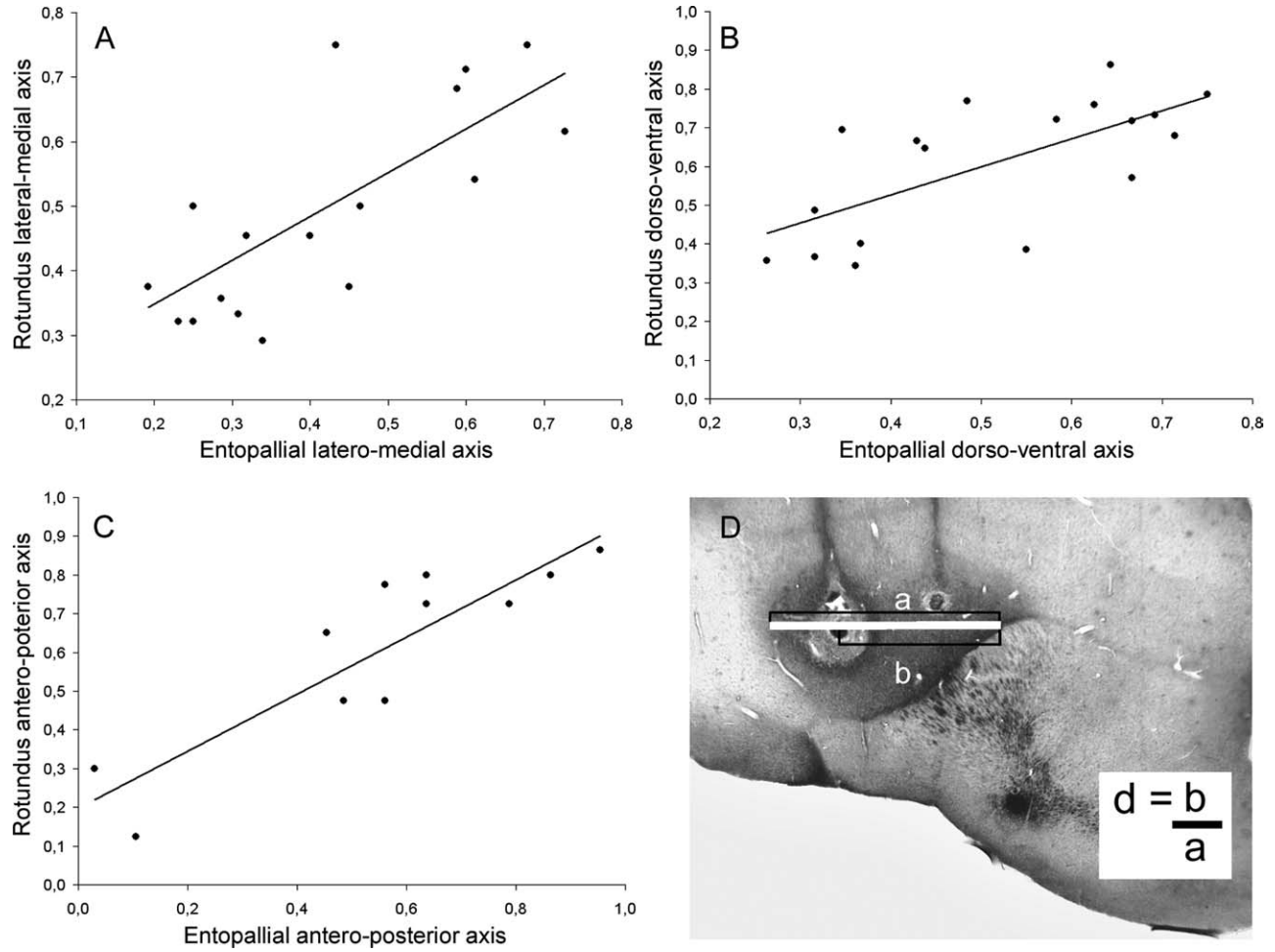

Figure 9. Correlation between the crystal position in the entopallium and the position of the labeled cell clusters in the Rt. **A–C**: Each plot correlates to the normalized position values of the crystals in the E and the normalized position values of the corresponding labeled cell cluster in the Rt. **D**: The photograph illustrates the procedure for position normalization. In this case, the distance from the center of the crystal to the medial border of the E (b) and the width of the E (a) were measured. The quotient between these two values corresponds to normalized distance of the crystal to the medial border of E (d). The same procedure was applied to the dorsomedial axis. For the rostrocaudal axis however, measurements of the approximate anteroposterior stereotaxis coordinates (Karten and Hodos, 1977) were used as points for the plots. Only the lineal regressions between the axes with significant correlation coefficients are shown. These graphs indicate that there is a topographic projection from Rt to the E that keeps the same three orthogonal axes.

In addition, if the pattern of entopallial anterograde label resulting from each of our single injections experiments is superimposed, it becomes evident that the rotundal terminals cover the complete entopallium, confirming the results of our multiple BDA injection experiment. Further, if the resulting entopallial labeling areas after the injections in the centralis subdivision are superimposed, and the area labeled after the injection in the posterior subdivision is subtracted, it highlights a central area whose shape matches well the shape of the central entopallial area suggested by the results of the BDA triple injection. This central area spans most of the ventral portion of E, and is characterized by a comparatively low density of rotundal terminals (Figs. 2B, 3D).

Our interpretation of these results is the following: The subdivision-specific rotundal afferents defines three different rostrocaudal partitions in the E: Anterior, Central, and Posterior. The anterior, drop-shaped zone is defined by high-density afferents from the dorsal-anterior subdivision of the Rt. The caudal zone is characterized by high-density afferents coming from the posterior rotundal subdivision; this entopallial zone is triangular in shape, and its longer side corresponds with the dorsocaudal boundary of E. Finally, the central zone is defined by the comparatively less dense afferents from the central rotundal subdivision (Fig. 11).

Point-to-point topography in the rotundo-entopallial projection

As stated above, previous studies in the rotundo-entopallial projection have shown a zonal, rostrocaudal segregation of the rotundal afferents onto E that was confirmed

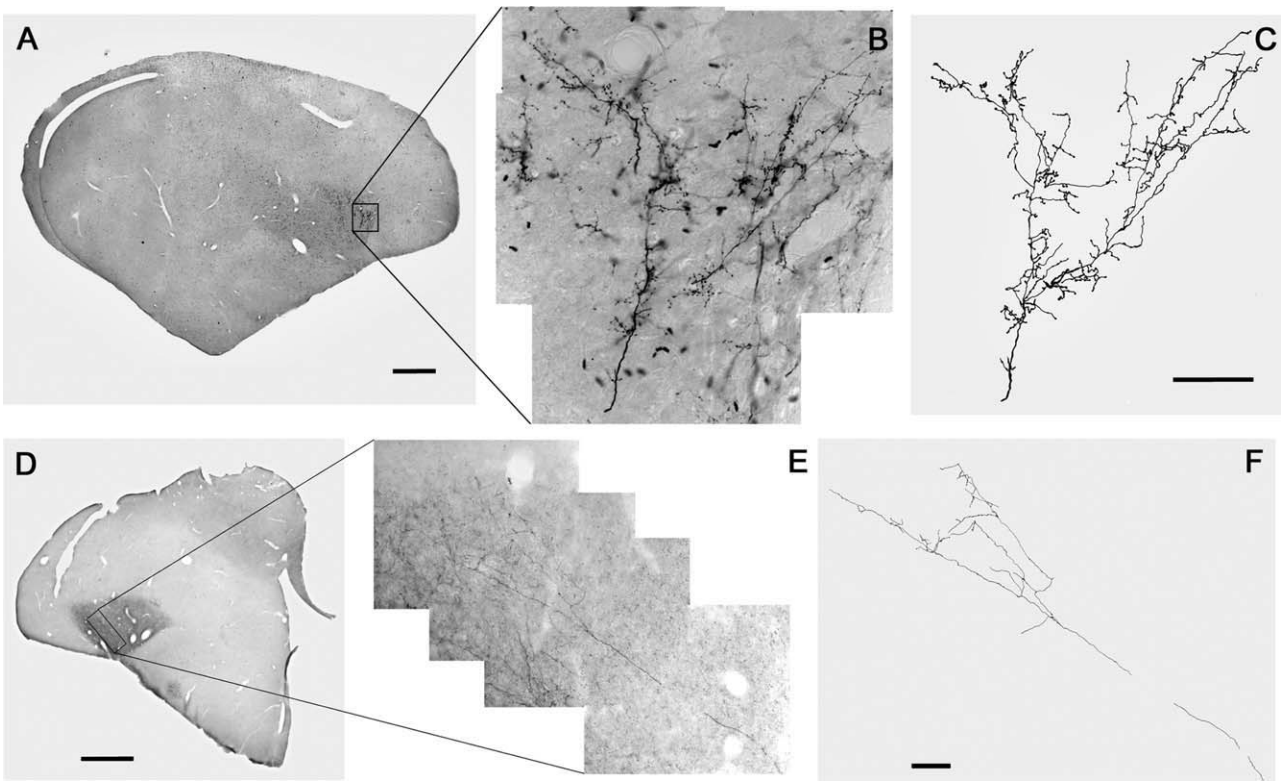

Figure 10. Reconstruction of two rotundal axon terminals in the E, after localized BDA injections in the nucleus rotundus. **A,D**: Low-power photographs of sagittal (A) and coronal (D) sections through the telencephalon showing the anterogradely labeled fibers in the entopallium. **B,E**: Higher-magnification photographs of the corresponding boxed areas on the left, each showing the morphology of one terminal fiber in the E. **C,F**: Camera lucida reconstruction of the terminal fibers, based in two contiguous sections of 60 μm. Note that the width of the branching area in both terminals is no larger than 150 μm. Scale bars, left = 1 mm; right: = 50 μm.

in the present study. In addition, we noticed that the BDA injections into the dorsal and ventral portions of the Rt-Ce result in segregated dorsal and ventral labeled areas within the central entopallial zone, suggesting a finer topography in the projection from Ce to its entopallial zone. We decided to investigate this possibility by injecting different retrograde tracers in their crystalline form, using a solid tracer microinjector (Marin et al., 2000). This technique allowed us to produce injection sites without superimposed diffusion halos, even when the crystals were less than 100 μm apart from each other. We found that simultaneous injections of two different tracers into one of the three rostrocaudal entopallial zones resulted in retrogradely labeled cells confined to one of the three rotundal subdivisions, further supporting the zonal topography previously described. Furthermore, we found that the retrogradely labeled cells were always grouped together forming two clusters, and that these clusters were located within the corresponding rotundal subdivision in such a way that their relative positions correlated well with the relative positions of the crystals in the entopallium.

Thus, these results strongly suggest a "point-to-point," topographical organization in the projection of each rotundal subdivision to its recipient entopallial zone. The results of the control experiments, as well as the quantitative spatial analysis of our data, further confirm these results, and indicate that the rotundo-entopallial map follows a direct topological arrangement. Interestingly, since the rotundal fibers enter the E from its ventral aspect, we cannot discount the possibility that our more ventral crystalline injections may have labeled some rotundal fibers terminating at more dorsal levels, thus leading to a more imprecise dorsoventral distinction of the retrogradely labeled cluster of cells inside Rt.

Taken together, these observations show that the anatomical organization of the rotundo-entopallial projection is much more fine and precise than previously appreciated. Furthermore, these results strongly suggest that, in the tectofugal pathway, a highly convergent stage (the tectorotundal projection) is followed by a highly topographic subsequent stage (the rotundo-entopallial projection). It is interesting to note that this pattern seems to be the general organization also for the descending streams of the tectofugal pathway (Hellmann et al., 2004).

Previous studies have shown that tectorotundal projections are highly convergent, in such a way that every

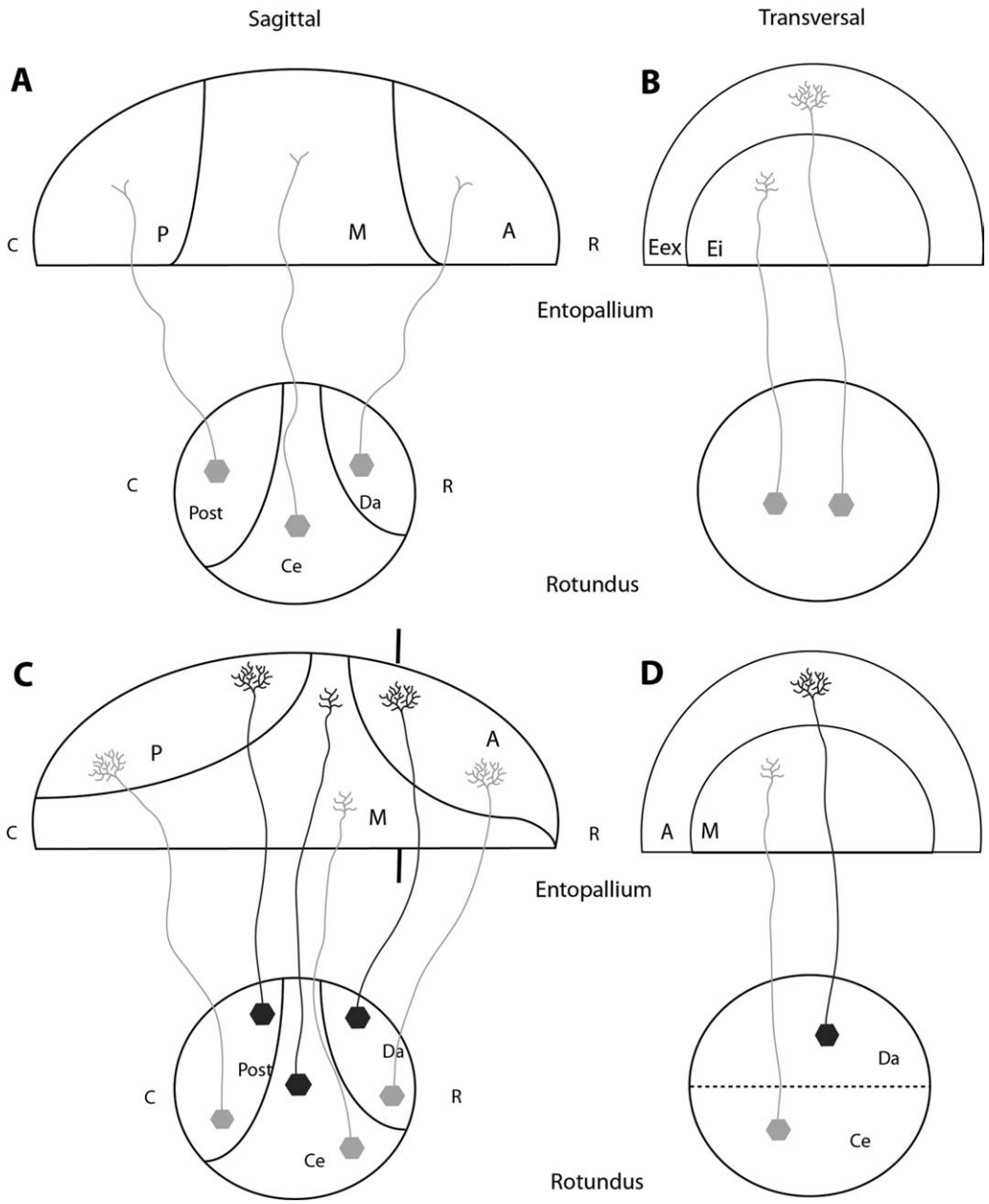

Figure 11. Schematic representations of three different rotundo-entopallial projections models. **A**: Zonal topography (Laverghetta and Shimizu, 2003). The rostrocaudal order of the rotundal subdivisions is maintained by the rotundo-entopallial projections. No topography inside each module is specified. **B**: The E is divided in internal and external divisions: E externus (Eex) and E internus (Ei) (Krützfeldt and Wild, 2005). The Eex is characterized by a comparative higher density of rotundal terminals than the Ei. It is not specified whether Eex and Ei are present throughout all rostrocaudal levels nor the rotundal origin of the afferences to Eex and Ei. **C**: Topographic arrangement proposed in the present study. The E has three main rotundal termination zones, each receiving the projections from the corresponding rotundal subdivisions. Each of the rotundo-entopallial subdivisions is topographically organized. As the rotundal terminations in the medial (M) entopallial zone are less dense than the anterior (A) and posterior (P) zones, the internal entopallial subdivision of Krützfeldt and Wild (2005) may correspond to our M zone. **D**: Hypothetical transversal sectioning at a rostral level indicated by the vertical lines in C showing how the differential terminal density observed in a transverse section by Krützfeldt and Wild (2005) could correspond to a composition of the projection from Da and Ce rotundal subdivisions.

visual locus in the Rt receives afferents from a subpopulation of tectal cells originating in all regions of the tectal surface (Marin et al., 2003). Accordingly, receptive fields of rotundal neurons are spatially gigantic (half or the entire contralateral hemifield; Morenkov and Pivovarov, 1975; Wang et al., 1993), and the receptive fields of these cells superimpose each other almost totally. This high degree of convergence seems to imply that the

relative spatial position of the rotundal cells is of no functional importance. However, according to our results, the spatial position of the rotundal neurons seems to be important, as the rotundus-entopallial projection follows a topographic pattern, through which the relative spatial position of each rotundal locus is replicated at the entopallial level. Furthermore, these results imply that the same array of tectal cells that drives the visual activity of a particular rotundal locus also drives the activity of the corresponding entopallial locus. The consequences of this anatomical arrangement on the spatial properties of the entopallial receptive fields become then very interesting, and deserve to be investigated further.

Projection pattern of nucleus triangularis

Nucleus triangularis has been distinguished as a valid rotundal subdivision in several previous studies (Benowitz and Karten, 1976; Mpodozis et al., 1996; Marin et al., 2003). However, in the present study we failed to identify an entopallial partition in receipt of projections from the Tr. Nucleus triangularis is a small target, and we were unable to perform tracer injections discrete enough as to compromise mainly this structure. Our crystalline tracer injections in the E, even when discrete, also failed to reveal a distinct entopallial region in receipt of Tr afferences. In fact, we found a discrete number of retrogradely labeled cells in Tr after all and each one of our crystalline injections, regardless of the location of the injection in the E (Figs. 4–8). These retrograde labeled cells were more numerous when the crystals were placed in the central entopallial partition than in the caudal or anterior portions (compare Figs. 4–8). These results suggest that nucleus triangularis project mainly to the central, but to all partitions of the entopallium, with no evident topographical order. A further detailed study of this issue will be necessary to clarify these observations.

Arborization of the rotundal fibers on the entopallium

The results of our double-injection and control experiments suggest that the rotundal terminal arborizations should span no further than 300 μm, since a 100-μm separation between the crystals results in a small proportion of double-labeled cells, while 500 μm of separation produce no double-labeled cells. Previous studies on the morphology of the rotundal axons in E have shown that they emit numerous varicosities and side branches. However, as these studies have been based on extracellular injections or the Golgi method (Tömböl et al., 1993; Egedi and Tömböl, 1993, 1994), they lack the precise descriptions of the morphology and arborization pattern of individual axons.

We also attempted to label the arborization of individual rotundal fibers by making small extracellular BDA injections into the Rt. Due to the limitations of this technique, we obtained only a few fibers distinguishable as individual axons. We observed that these axons enter the E by its ventral base, and follow mainly a dorsoventrally oriented course. The ventral segment of these axons was devoid of ramifications and varicosities. Once the axons progressed dorsally, they began to arborize profusely in thinner branches, which finally arborized again in processes that exhibited a high density of varicosities. These varicosities are most probably synaptic buttons, as previously demonstrated by electron microscopy (Tömböl et al., 1993; Egedi and Tömböl, 1994). This implies that even when the axons follow a course of several hundreds microns inside the E, their synaptic domains are restricted to their terminal branches. In our cases, the size of these branching regions (major axis) does not exceed 150 μm, which is in close agreement with the results of our double-injection experiments. However, due to the limited nature of our sample, these results require a more thorough validation. Intracellular filling of cells in the different rotundal subdivisions may be required to yield a complete and reliable map of the rotundal fiber morphology in the E.

Anatomic divisions in the entopallium: rostrocaudal versus dorsoventral partitions

In an attempt to reveal possible anatomical subdivisions in the E, Krützfeldt and Wild (2005) performed large injections of BDA in the Rt. Their results support the existence of a rostrocaudal zonation of the rotundal afferents to the E, as previously demonstrated by Laverghetta and Shimizu (2003). In addition, they also propose a dorsoventral partition of the E in two layers: internal (ventral) and an external (dorsal), distinguishable by a differential pattern of labeling of the rotundal afferents (higher density in the E external), and by the presence in the E internal of a relatively dense population of parvalbumin positive neurons (but note this last pattern is inverted in the zebrafinch entopallium; Krützfeldt and Wild, 2004). Furthermore, the E internal appears to be reciprocally connected with the mesopallial MVL, and also seems to be the sole source of entopallial projections to the lateral striatum.

Our results, however, show that the rostral and caudal entopallial zones receive at their full dorsoventral extent a homogeneous density of projections from the rotundus, suggesting that the internal–external partition is not present at these entopallial levels. Similarly, we found that the central entopallial zone also presents a

homogeneous, but less dense, distribution of rotundal afferent fibers (Fig. 2B).

These discrepancies could be partially due to the different plane of brain sectioning used in these studies. Krützfeldt and Wild (2004, 2005) processed their material in the transverse plane, while in the present study we used transverse as well as sagittal sectioning. This is a significant difference, because it is the sagittal, but not the transverse sectioning that allows the visualization of the full rostrocaudal profile of E, thereby making possible a direct observation of the shape and extent of the rostrocaudal regions defined by the rotundal afferents. Taking this into account, and considering that Krützfeldt and Wild (2005) did not indicate whether their internal–external partition was present at all rostrocaudal levels of the E, we think that a way to reconcile these discrepancies is to propose that our central E region corresponds to the E internal proposed by Krützfeldt and Wild (2005). Both the central (present study) and internal (Krützfeldt and Wild, 2005) divisions share the shape, the extension, and a relatively minor density of rotundal terminals (Figs. 2B, 3D). Similarly, we propose that the external subdivision of Krützfeldt and Wild (2005) corresponds to the dorsal caps of our anterior and posterior regions (Fig. 11). In other words, we propose that the entopallium externum of Krützfeldt and Wild (2005) is in receipt of rotundal afferences that mainly derive from the dorsal-anterior and posterior subdivisions, while the E internum receives rotundal afferences mainly from the centralis subdivision. Validation of this proposition will require further detailed studies, starting with a more precise description of the morphology of rotundal terminals in each of the entopallial regions.

Parallel pathways in the tectofugal system

As stated in the introduction, several anatomical and physiological studies have shown that each of the rotundal divisions receives afferents from different populations of tectal ganglion cells, and that cells in these subdivisions are selectively activated by different visual attributes (Wang et al., 1993). These segregations seem to be of functional significance, since selective lesion studies indicate that the rostral and caudal rotundal subdivisions are differentially involved in visual discriminations (Laverghetta and Shimizu, 1999). Such differential involvement persists at the entopallial level, as behavioral studies indicate that rostral and caudal zones of the entopallium have a differential role in visual discriminations (Nguyen et al., 2004). Taken together, these results indicate that the tectofugal system of birds is composed of at least three independent channels (although probably more channels are present; see Hellmann and Gunturkun, 2001), through which different aspects of visual operations are segregated. In this view, the rostral, medial, and caudal divisions of the entopallium we illustrate here can be regarded as the pallial stages of this segregated organization. Furthermore, the topographic arrangement we have found in the rotundo-entopallial projections seems to indicate that the functional segregation of the tectofugal system that originates at the rotundal stage is preserved at the pallial stage. However, physiological studies have shown that the receptive fields of entopallial cells do not simply replicate the visual properties of rotundal neurons. In particular, entopallial neurons responded selectively to moving bars, preferring those moving parallel to their longest axis and have receptive fields with oddly defined borders (Engelage and Bishop, 1996). Thus, the entopallium cannot be considered simply as a telencephalic relay of the tectofugal system. The nature of the visual operations that take place at the entopallium then becomes very interesting and deserves to be thoroughly investigated from the perspective of the functional segregations that take place in the tectofugal system.

On the other hand, the ascending tectofugal parallel streams seem to depart subsequent to the entopallial level. Krützfeldt and Wild (2005) have shown that the internal E division, or, according to us, the medial entopallial subdivision, is the sole source of projections to the pallial MVL. The projection areas of the posterior and rostral divisions of the E are at present not clear, but it is likely that they may generate similar patterns of termination in other pallial areas, each performing as functional mirror images of the corresponding entopallial subdivision. Interestingly, this pattern of multiple visual pallial areas that start to emerge from this and previous studies resembles the organization of the mammalian visual extrastriate cortex, where a complete map of the visual space can be detected physiologically in many restricted areas, each of which is selectively sensitive to a different visual attribute, such as movement, color, luminance, etc. (Nassi and Callaway, 2009). Thus, future studies are required to better understand the organization of the entopallium efferents, focusing on the identification of the different visual streams that seem to depart from the E. The convergence of these visual streams in higher association or premotor areas is of particular interest, and could give important clues about the generation of the complex visually guided behaviors exhibited by birds.

ACKNOWLEDGMENTS

We thank Dr. Martin Wild for critical comments and helpful assistance in the preparation of the article. We also thank Dr. Harvey Karten for intellectual support. We thank Elisa Sentis and Solano Henriquez for technical assistance.

LITERATURE CITED

Benowitz LI, Karten HJ. 1976. Organization of the tectofugal pathway in the pigeon: a retrograde transport study. J Comp Neurol 167:503–520.

Bessette BB, Hodos W. 1989. Intensity, color, and pattern discrimination deficits after lesions of the core and belt regions of the ectostriatum. Vis Neurosci 2:27–34.

Brauth SE, Kitt CA, Reiner A, Quirion R. 1986. Neurotensin binding sites in the forebrain and midbrain of the pigeon. Brain Res 253:358–373.

Butler AB. 1994. The evolution of the dorsal thalamus of jawed vertebrates, including mammals: cladistic analysis and a new hypothesis. Brain Res Brain Res Rev 19:29–65.

Butler AB, Hodos W. 2005. Comparative vertebrate neuroanatomy: evolution and adaptation. Hoboken, NJ: John Wiley & Sons.

Cohen DH. 1967. The hyperstriatal region of the avian forebrain: a lesion study of possible functions, including its role in cardiac and respiratory conditioning. J Comp Neurol 131:559–570.

Dietl MM, Palacios JM. 1988. Neurotransmitter receptors in the avian brain. I. Dopamine receptors. Brain Res 439:354–359.

Dietl MM, Corte's R, Palacios JM. 1988a. Neurotransmitter receptors in the avian brain. II. Muscarinic cholinergic receptors. Brain Res 439:360–365.

Dietl MM, Corte's R, Palacios JM. 1988b. Neurotransmitter receptors in the avian brain. I. GABA-benzodiazepine receptors. Brain Res 439:366–371.

Egedi Gy, Tömböl T. 1993. A phaseolus lectin anterograde tracing study of the rotundotelencephalic projections in the domestic chick. J Hirnforsch 34:317–333.

Egedi Gy, Tömböl T. 1994. EM study on terminals labelled by phaseolus vulgaris lectin in ectostriatum peripheriсum and neostriatum intermedium. J Hirnforsch 35:405–414.

Engelage J, Bischof HJ. 1996. Single cell responses in the ectostriatum of the zebra finch. J Comp Physiol [A] 179:785–795.

Frost BJ, DiFranco DE. 1976. Motion characteristics of single units in the pigeon optic tectum. Vision Res 16:1229–1234.

Granda AM, Yazulla S. 1971. The spectral sensitivity of single units in the nucleus rotundus of pigeon, Columba livia. J Gen Physiol 57:363–384.

Gu Y, Wang Y, Zhang T, Wang SR. 2002. Stimulus size selectivity and receptive field organization of ectostriatal neurons in the pigeon. J Comp Physiol [A] 188:173–178.

Hellmann B, Waldmann C, Güntürkün O. 1995. Cytochrome oxidase activity reveals parcellations of the pigeon's ectostriatum. Neuroreport 6:881–885.

Hellmann B, Güntürkün O. 2001. Structural organization of parallel information processing within the tectofugal visual system of the pigeon. J Comp Neurol 429:94–112.

Hellmann B, Güntürkün O, Manns M. 2004. Tectal mosaic: organization of the descending tectal projections in comparison to the ascending tectofugal pathway in the pigeon. J Comp Neurol 472:395–410.

Hodos W, Karten HJ. 1966. Brightness and pattern discrimination deficits in the pigeon after lesions of nucleus rotundus. Exp Brain Res 2:151–167.

Hodos W, Karten HJ. 1970. Visual intensity and pattern discrimination deficits after lesions of ectostriatum in pigeons. J Comp Neurol 140:53–68.

Hodos W, Bonbright JC. 1974. Intensity difference thresholds in pigeons after lesions of the tectofugal and thalamofugal visual pathways. J Comp Physiol Psychol 87:1013–1031.

Hodos W, Karten HJ. 1974. Visual intensity and pattern discrimination deficits after lesions of the optic lobe in pigeons. Brain Behav Evol 9:165–194.

Hodos W, Macko KA, Bessette BB. 1984. Near-field acuity changes after visual system lesions in pigeons. II. Telencephalon. Behav Brain Res 13:15–30.

Hodos W, Weiss SR, Bessette BB. 1986. Size-threshold changes after lesions of the visual telencephalon in pigeons. Behav Brain Res 21:203–214.

Hodos W, Weiss SR, Bessette BB. 1988. Intensity difference thresholds after lesions of ectostriatum in pigeons. Behav Brain Res 30:43–53.

Husband SA, Shimizu T. 1999. Efferent projections of the ectostriatum in the pigeon (*Columba livia*). J Comp Neurol 406:329–345.

Jassik-Gerschenfeld D, Guichard J. 1972. Visual receptive fields of single cells in the pigeon's optic tectum. Brain Res 40:303–317.

Karten HJ, Revzin AM. 1966. The afferent connections of the nucleus rotundus in the pigeon. Brain Res 2:368–377.

Karten HJ, Hodos W. 1967. A stereotaxic atlas of pigeon brain (*Columba livia*). Baltimore: Johns Hopkins Press.

Karten HJ, Hodos W. 1970. Telencephalic projections of the nucleus rotundus in the pigeon (*Columba livia*). J Comp Neurol 140:35–51.

Karten HJ, Cox K, Mpodozis J. 1997. Two distinct populations of tectal neurons have unique connections within the tectorotundal pathway of the pigeon (*Columba livia*). J Comp Neurol 387:449–465.

Kertzman C, Hodos W. 1988. Size-difference thresholds after lesions of thalamic visual nuclei in pigeons. Vis Neurosci 1:83–92.

Kimberly RP, Holden AL, Bamborough P. 1971. Response characteristics of pigeon forebrain cells to visual stimulation. Vision Res 11:475–487.

Krützfeldt NOE, Wild JM. 2004. Definition and connections of the entopallium in the zebra finch (*Taeniopygia guttata*). J Comp Neurol 468:452–465.

Krützfeldt NO, Wild JM. 2005. Definition and novel connections of the entopallium in the pigeon (*Columba livia*). J Comp Neurol 490:40–56.

Laverghetta AV, Shimizu T. 1999. Visual discrimination in the pigeon (*Columba livia*): effects of selective lesions in the nucleus rotundus. Neuroreport 10:981–985.

Laverghetta AV, Shimizu T. 2003. Organization of the ectostriatum based on afferent connections in the zebra finch (Taeniopygia guttata). Brain Res 963:101–112.

Macko KA, Hodos W. 1984. Near-field acuity after visual system lesions in pigeons. I. Thalamus. Behav Brain Res 13:1–14.

Marin G, Henny P, Letelier JC, Sentis E, Karten H, Mrosko B, Mpodozis J. 2001. A simple method to microinject solid neural tracers into deep structures of the brain. J Neurosci Methods 106:121–129.

Marin G, Letelier JC, Henny P, Sentis E, Farfan G, Fredes T, Pohl N, Karten HJ, Mpodozis J. 2003. Spatial organization of the pigeon tectorotundal pathway: an interdigitating topographic arrangement. J Comp Neurol 458:361–380.

Martinez-de-la-Torre M; Martinez S; Puelles L. 1990. Acetylcholinesterase-histochemical differential staining of subdivisions within nucleus rotundus in the chick. Anat Embryol 181:129–135.

Morenkov EDPivovarov A. 1975. Reactions of neurons of dorsal and ventral thalamus of tortoise Emys orbicularis to visual stimuli. J Evol Biochem Physiol 11:56–61.

Mpodozis J, Cox K, Shimizu T, Bischof HJ, Woodson W, Karten HJ. 1996. GABAergic inputs to the nucleus rotundus (pulvinar inferior) of the pigeon (*Columba livia*). J Comp Neurol 374:204–222.

Nassi JJ, Callaway EM. 2009. Parallel processing strategies of the primate visual system. Nat Rev Neurosci 10:360–372.

Nguyen AP, Spetch ML, Crowder NA, Winship IR, Hurd PL, Wylie DRW. 2004. A dissociation of spatial-pattern vision in the avian telencephalon: implications for the evolution of "visual streams." J Neurosci 24:4962–4970.

Nixdorf BE, Bischof HJ. 1982. Afferent connection of the ectostriatum and visual wulst in the zebrafinch (*Taenopygia guttata castonotis* Gould): an HRP study. Brain Res 248:9–17.

Redies C, Ast M, Nakgawa S, Takeichi M, Martinez-de-la-Torre M, Puelles L. 2000. Morphological fate of diencephalic prosomeres and their subdivisions revealed by mapping cadherin expression. J Comp Neurol 421:481–514.

Rehkamper G, Zilles K, Schleicher A. 1985. A quantitative approach to cytoarchitectonics. X. The areal pattern of the neostriatum in the domestic pigeon, Columba livia f.d. A cyto- and myeloarchitectonical study. Anat Embryol 171:345–355.

Reiner A, Perkel DJ, Bruce LL, Butler AB, Csillag A, Kuenzel W, Medina L, Paxinos G, Shimizu T, Striedter G, Wild M; Ball GF, Durand S, Günturkün O, Lee DW, Mello CV, Powers A, White AS, Hough G, Kubikova L, Smulders TV, Wada K, Dugas-Ford J, Husband S, Yamamoto K, Yu J, Siang C, Jarvis ED. 2004. Revised nomenclature for avian telencephalon and some related brainstem nuclei. J Comp Neurol 473:377–414.

Revzin AM. 1970. Some characteristics of wide-field units in the brain of the pigeon. Brain Behav Evol 3:195–204.

Tömböl T. 1991. Arborization of afferent fibers in ectostriatum centrale. Golgi study. J Hirnforsch 32:563–575.

Tömböl T, Magloczky Zs, Stewart MG, Csillag A. 1988. The structure of chicken ectostriatum. I. Golgy study. J Hirnforsch 29:525–546.

Tömböl T, Egedi G, Németh A. 1993. EM study on Phaseolus vulgaris lectin labelled terminals of rotundal fibers and on GABA immunogold stained structures in chicken ectostriatum centrale. J Hirnforsch 34:517–537.

Veenman CL, Reiner A. 1994. The distribution of GABA-containing perikarya, fibers, and terminals in the forebrain and midbrain of pigeons, with particular reference to the basal ganglia and its projection targets. J Comp Neurol 339:209–250.

Veenman CL, Albin RL, Richfield EC, Reiner A. 1994. Distributions of GABA a, GABA b, and benzodiazepine receptors in the forebrain and midbrain of pigeons. J Comp Neurol 344:161–189.

Wang Y, Frost BJ. 1992. Time to collision is signalled by neurons in the nucleus rotundus of pigeons. Nature 356: 236–238.

Wang YC, Jiang S, Frost B. 1993. Visual processing in pigeon nucleus rotundus: luminance, color, motion and looming subdivisions. Vis Neurosci 10:21–30.

Watanabe S. 1991. Effects of ectostriatal lesions on natural concept, pseudoconcept, and artificial pattern discrimination in pigeons. Vis Neurosci 6:497–506.

Watanabe S. 1992. Effect of lesions in the ectostriatum and Wulst on species and individual discrimination in pigeons. Behav Brain Res 49:197–203.

Watanabe M, Ito H, Ikushima M. 1985. Cytoarchitecture and ultraestructure of the avian ectostriatum: afferent terminals from the dorsal telencephalon and some nuclei in the thalamus. J Comp Neurol 236:241–257.

Yazulla S, Granda AM. 1972. Localization of visual structure in the diencephalon of pigeon (*Columba livia*). Vision Res 12: 1933–1936.